Polymer Degradation and Stability 98 (2013) 1439–1449

Contents lists available at SciVerse ScienceDirect

Polymer Degradation and Stability

journal homepage: www.elsevier.com/locate/polydegstab

Melt compounding of poly (3-hydroxybutyrate-*co*-3-hydroxyvalerate)/nanofibrillated cellulose nanocomposites

Yottha Srithep [a,b], Thomas Ellingham [b], Jun Peng [b], Ronald Sabo [c], Craig Clemons [c], Lih-Sheng Turng [b,*], Srikanth Pilla [b]

[a] Faculty of Engineering, Mahasarakham University, Khamriang, Kantarawichai, Mahasarakham Province, 44150, Thailand
[b] Polymer Engineering Center, Department of Mechanical Engineering, University of Wisconsin–Madison, Madison, WI 53706, USA
[c] USDA Forest Service, Forest Products Laboratory, Madison, WI 53726, USA

ARTICLE INFO

Article history:
Received 15 December 2012
Received in revised form
25 April 2013
Accepted 2 May 2013
Available online 13 May 2013

Keywords:
Nanofibrillated cellulose (NFC)
Poly(3-hydroxybutyrate-*co*-3-hydroxyvalerate) (PHBV) nanocomposites
Mechanical and thermal properties
Carbon dioxide solubility and foaming
Thermal stability and degradation

ABSTRACT

Using natural cellulosic fibers as fillers for biodegradable polymers can result in fully biodegradable composites. In this study, biodegradable nanocomposites were prepared using nanofibrillated cellulose (NFC) as the reinforcement and poly (3-hydroxybutyrate-*co*-3-hydroxyvalerate, PHBV) as the polymer matrix. PHBV powder was dispersed in water, mixed with an aqueous suspension of NFC fiber, and freeze-dried. The resulting PHBV/15 wt% NFC was then used as a master batch in a subsequent melt compounding process to produce nanocomposites of various formulations. Its properties such as its mechanical properties, crystallization behavior, solubility of carbon dioxide (CO_2), foaming behavior, and thermal stability and degradation of PHBV due to NFC were evaluated. Scanning electron microscopy (SEM) and transmission electron microscopy (TEM) were used to study the dispersion of NFC fibers. Adding NFC increased the tensile modulus of the PHBV/NFC nanocomposites nearly twofold. Differential scanning calorimetry (DSC) analysis showed that the NFC served as a nucleating agent, promoting the early onset of crystallization. However, high NFC content also led to greater thermal degradation of the PHBV matrix. Dynamic mechanical analysis (DMA) showed an increase of the storage modulus in the glassy state with increasing NFC content, but a more significant increase in modulus was detected above the glass transition temperature. The solubility of CO_2 in the PHBV/NFC nanocomposites decreased and the desorption diffusivity increased as more NFC was added. Finally, the foaming behavior of PHBV/NFC nanocomposites was studied and the addition of NFC was found to inhibit foaming.

© 2013 Elsevier Ltd. All rights reserved.

1. Introduction

The development of commercially viable biodegradable plastics is an important effort in preserving and revitalizing our global environment and economy. Polyhydroxyalkanoates (PHAs) have attracted much attention over the last two decades mainly due to increasing environmental concerns and the realization that our petroleum resources are finite [1,2]. PHAs have received a great deal of research interest because their mechanical performance is similar to petroleum-based polymers such as polypropylene (PP) [3]. PHAs, which also include poly(3-hydroxybutyrate) (PHB) and copolymer poly(3-hydroxybutyrate-*co*-3-hydroxyvalerate) (PHB/HV), are a family of polyesters that are synthesized and intracellularly accumulated as a carbon and energy storage material in various microorganisms [4]. Generally, PHB/HV (or PHBV) is less crystalline and more flexible than the highly crystalline and relatively brittle and hydrophobic PHB [5].

Reinforcing fibers of various sizes and forms—e.g., natural plant fibers (cellulose fibers), glass fibers, carbon fibers, carbon nanotubes, etc. —have been effectively used in polymer composites as reinforcing agents [3]. Nanofillers, however, are found to be preferable in many applications due to their high surface area-to-volume ratios, lower concentrations needed to achieve reinforcing effects, and the ability to potentially improve toughness along with strength and stiffness. Nanofibrillated cellulose (NFC), a biologically derived nanofiber reinforcement suitable for polymeric materials, is an interconnected web with fibrils having a diameter in the range of 10–50 nm [6]. Although NFC has numerous advantages, which include low density, renewability, high specific properties, biodegradability, gas barrier properties, and derivation from abundant natural resources, the processing temperatures for these materials are restricted to about 200 °C due to degradation beyond this

* Corresponding author. Tel.: +1 608 262 0586; fax: +1 608 265 2316.
E-mail addresses: turng@engr.wisc.edu, turng@wid.wisc.edu (L.-S. Turng).

0141-3910/$ – see front matter © 2013 Elsevier Ltd. All rights reserved.
http://dx.doi.org/10.1016/j.polymdegradstab.2013.05.006

temperature [7–9]. Another drawback of using NFC is the difficulty in dispersing them uniformly in a non-polar medium because of their polar surface [10]. Therefore, the use of NFC in nanocomposites has mainly been limited to aqueous or polar environments and the processing techniques have been limited to the laboratory scale. Thus, it will be important to develop new processing techniques which can be scaled up and used industrially.

It is well known that when a low molecular weight compound, such as carbon dioxide, comes into contact with a polymer, sorption of the low molecular weight specie by the polymer occurs. Carbon dioxide at high pressure can be dissolved in a polymeric matrix [11]. The use of CO_2 as a solvent or physical blowing agent offers the possibility to develop new "clean and environmental friendly" techniques for polymer processing and foams. It is therefore of interest in this study to measure the solubility of CO_2 in PHBV and PHBV/NFC nanocomposites.

Polymeric foams find application as materials for thermal and acoustic insulation, energy dissipation, shock protection, packaging, etc. [12]. Polymeric foams are light weight and offer better thermal insulation compared to solid materials. This study also carried out batch foaming experiments using CO_2 as a physical blowing agent to investigate the influence of NFC on the foaming behavior of PHBV/NFC nanocomposites.

It is hoped that the resulting biobased and biodegradable PHBV/NFC nanocomposites may find many potential applications in the fields of structural components, packaging, and biomedical devices [13,14]. Various characterization techniques analyzing mechanical, morphological, and thermal properties were employed to characterize the PHBV/NFC nanocomposites. Moreover, the solubility of carbon dioxide was measured and the foaming properties of PHBV and PHBV/NFC nanocomposites were evaluated.

2. Experiments

2.1. Materials

The materials used in this study were PHBV powder and NFC. PHBV powder under the trade name Y1000 was purchased from Ningbo Tianan Biologic Material Co. Ltd. (Tinan-ENMAT, China). The percentage of HV in the PHBV copolymer (Y1000) was 3%.

NFC was prepared according to a procedure described by Saito and Isogai [15]. In particular, fully bleached Kraft eucalyptus fibers were oxidized with sodium hypochlorite using tetramethylpiperidine-1-oxy radical (TEMPO) sodium bromide as a catalyst. The TEMPO-mediated oxidation was carried out at a pH of 10 at 25 °C for 3 h. The fibers were then thoroughly washed and refined in a disk refiner with a gap of approximately 200 μm. The coarse fibers were separated by centrifuging at a force of 12,000 G, and the nanofiber dispersion was concentrated to 1% using ultrafiltration. A final clarification step was performed in which the nanofiber dispersion was passed once through an M-110EH-30 microfluidizer (Microfluidics, Newton, MA) with 200 μm and 87 μm chambers in series. An aqueous suspension of NFC fibers at 0.4 wt% was obtained and used in this study.

2.2. Sample preparation

Composites were prepared using a two-step process. Masterbatch preparations using a freeze drier were followed by melt compounding, as described below.

2.2.1. Preparation of the masterbatch

PHBV powder was first dispersed in distilled water, stirred for 1 h, and then mixed with an aqueous suspension of NFC to reach a dry weight ratio between PHBV and NFC of 85:15 (15% NFC). The mixture was then stirred overnight using a magnetic stirrer. To prepare the composites, the water medium had to be removed from the corresponding aqueous suspension of NFC while the NFC fibers remained fully dispersed. Hence, the suspension was quickly frozen by liquid nitrogen to prevent the PHBV powder from settling. In addition, rapid freezing might avoid NFC aggregation during freeze drying, as report by Pääkkö et al. [16]. The frozen mixture was then freeze-dried using a 4.5 L Labconco FreeZone freeze drier to remove the water thoroughly. The dried PHBV + 15% NFC masterbatch was later diluted to 2.5, 5, and 10 wt% NFC content by melt compounding, as described below.

2.2.2. Melt compounding and preparation of specimens

PHBV composites with 0, 2.5, 5, and 10 wt% NFC content were prepared by melt compounding of the PHBV powders and the NFC masterbatch. PHBV was dried in an oven for 2 h at 90 °C before processing and melt compounding was done using a thermokinetic mixer (K-mixer). The nanocomposites were then compounded in 50 g batches and discharged when the temperature reached 180 °C. There was no external heating source in the K-mixer besides frictional (viscous) heating and the compounding process was completed in less than 2 min. This short heating/mixing time reduced the potential for thermal degradation. The K-mixer's rotor speed was set at 6000 rpm. After discharge, the molten nanocomposite was subsequently granulated. Tensile bars (ASTM D638 Type V, 63.5 mm by 3.2 mm by 1.6 mm), flexural specimens (nominal dimensions of 125.0 mm by 12.7 mm by 3.2 mm), and rectangular specimens (nominal dimensions of 25 mm by 25 mm by 1.2 mm) with the same dimension for both neat and nanocomposites were injection molded using a micro injection molding machine (DSM Xplore, Geleen, The Netherlands). The molding was done at 180 °C with a mold temperature of 25 °C, a cooling time of 15 s, and a holding pressure of 7 bars.

2.3. Material characterization

2.3.1. Tensile testing

Tensile tests were performed on the injection molded tensile specimens following the ASTM D638 standard [17]. The static tensile modulus, strength, and strain-at-break were measured at room temperature (25 °C) and atmospheric conditions (relative humidity of 50 ± 5%) on an Instron 5865 mechanical testing instrument. The tensile tests were performed on all specimens using an initial load of 0.5 N and a constant crosshead speed of 1 mm/min. Five specimens of each sample group were tested and the average results were reported.

2.3.2. Scanning electron microscopy (SEM)

SEM images were examined using an SEM (JEOL Neoscope Benchtop) operated at 10 kV. All specimens were sputter-coated with a thin layer of gold (~20 nm) prior to examination.

2.3.3. Differential scanning calorimetry (DSC)

A differential scanning calorimeter (Q20 TA Instruments) was used to study the thermal properties of the nanocomposites. Specimens of 5–10 mg were placed in aluminum sample pans and heated from −50 °C to 210 °C at a 10 °C/min heating rate and held for 3 min at 210 °C to erase any prior thermal history before cooling at a rate of 10 °C/min to a temperature of −50 °C. The specimens were then reheated to 210 °C and cooled down to room temperature using the same heating and cooling rates of 10 °C/min. The crystallization temperature (T_c), melting temperature (T_m), and apparent melting enthalpy (ΔH_f) were determined from the DSC curves.

The absolute degree of crystallinity (χ_c) of the PHBV phase was calculated by

$$\chi_c(\%) = \frac{\Delta H_f(\text{PHBV})}{\Delta H^\circ(\text{PHBV})} \times \frac{100}{w} \quad (1)$$

where ΔH°(PHBV) is the enthalpy of melting per gram of 100% crystalline (perfect crystal; 109 J/g) and w is the weight fraction of PHBV in the nanocomposites [2].

2.3.4. Polarized optical microscopy (POM)

Crystallization behavior of the samples was studied by a Leitz SM-Lux POM. Microtomed PHBV/NFC nanocomposite specimens from the injection molded samples were sandwiched between two glass slides and heated to 230 °C. The specimens were equilibrated for 3 min to eliminate any residual PHBV crystallization seeds and then cooled down slowly to room temperature. Images of PHBV spherulites were taken by an attached digital camera.

2.3.5. Gel permeation chromatography (GPC)

The number- and weight-average molecular weights (M_n and M_w, respectively) and the polydispersity index (PDI; calculated as the ratio of M_w/M_n) for injection molded PHBV/NFC samples were determined by gel permeation chromatography (GPC). Specimens weighing 7.5 mg were dissolved in 3 mL of HPLC-grade chloroform via continuous stirring in a constant temperature sand bath (60 °C) for 1 h. The dissolved solution was filtered through a 0.2 μm PTFE membrane filter. For the PHBV-NFC samples, NFC which was not dissolved in chloroform was removed from the solutions by filtration. The filtration process was done in two stages: (1) using a standard filter paper and (2) using the 0.2 μm PTFE membrane filter. With an eluent flow rate of 1.0 mL/min, 100 mL specimens were injected into a Viscotek model VE2001 with Model 302-050 tetra detector array (differential refractive index (RI)). The system was calibrated using polystyrene standards.

2.3.6. Thermogravimetric analysis (TGA)

Specimens used for thermogravimetric analysis (TGA) were first dried at 90 °C for 2 days prior to testing. TGA was performed using a TGA Q50 (TA Instruments) from 25 to 600 °C at a heating rate of 10 °C/min. Approximately 10 mg of neat PHBV, neat NFC, or nanocomposites of various NFC content were used for each test. The weight loss was recorded and normalized against the initial weight.

2.3.7. Dynamic mechanical analysis (DMA)

Dynamic mechanical analysis measurements were performed on a DMA Q800 (TA instrument) in single cantilever mode. The dimensions of the rectangular specimen were 17.6 mm by 12.7 mm by 3.2 mm, which were cut from injection molded samples. During the DMA test, the specimens were heated at a rate of 3 K/min from −30–120 °C with a frequency of 1 Hz and a strain of 0.02%, which was in the linear viscoelastic region as determined by a strain sweep.

2.3.8. Absorption and desorption measurements

The main purpose of the absorption and desorption experiments was to establish the amount of CO_2 absorbed in the PHBV and PHBV/NFC nanocomposites (or gas solubility) and the rate of gas diffusivity (or gas diffusivity), which are important factors in the gas foaming process [18,19]. The original weights of these samples were measured using a digital balance readable to 0.0001 g. Absorption of CO_2 was facilitated by placing the specimens in a high pressure vessel under a CO_2 gas pressure of 5.52 MPa (800 psi) at room temperature. Afterward, the vessel was depressurized and the CO_2 absorbed specimens were removed from the pressure vessel and placed on a balance to record the CO_2 sorption in the pressure chamber (weight gain). The process of depressurization and removing the samples from the pressure chamber and weighing them took around 40 s. As soon as no further weight gain was recorded, the desorption process was carried out immediately to determine the amount of gas lost from the sorption curves. The diffusivities (D) for absorption and the desorption were derived as follows [20,21]:

$$D = \frac{\pi}{16}\left[\frac{d\left(\frac{M_t}{M_\infty}\right)}{d\left(\frac{\sqrt{t}}{l}\right)}\right]^2 \quad (2)$$

where M_t is the amount of gas lost at time t, M_∞ is the mass uptake at infinite time, and l is the thickness of the sample.

2.4. Foam preparation

To produce foamed structures in PHBV and PHBV/NFC nanocomposites, the CO_2-saturated samples were subjected to a rapid pressure drop and a rapid temperature increase that resulted in the nucleation and growth of gas nuclei. This was achieved by taking the samples out of the pressure chamber and heating them in a hot oil bath. The rapid decompression and rapid heating induced a sudden gas solubility drop in the samples [22]. This sudden drop of gas solubility created a thermodynamic instability in the gas/polymer solution, which caused the microcells to nucleate. Once the cells nucleated, they continued to grow until the material solidifies or the gas concentration drops below the solubility level [18].

3. Results and discussions

3.1. Freeze-dried aqueous suspension of NFC

The SEM images of PHBV powder, freeze-dried NFC, and freeze-dried masterbatch of PHBV + 15% NFC are shown in Fig. 1(a)–(c), respectively. As shown in Fig. 1(a), the individual PHBV powder is smaller than 1 μm. Freeze-dried NFC (Fig. 1(b)) shows an interconnected fibrillar skeleton structure with diameters on the order of 1 μm, although some of the nanofibers aggregated to form essentially 2-dimensional extended sheet-like structures. The observed fibrillar diameter after freeze drying was much larger than what was observed (e.g., 5–10 nm) in aqueous gels using a transmission electron microscopy (TEM, LEO 912) which a drop of dilute NFC solution was deposited on a carbon-coated TEM grid and allowed to dry prior to imaging (Fig. 1(d)). This indicates that some aggregation of the nanofibers took place in the process of freeze drying. Similar behavior in freeze drying results has been reported in another study [16]. For the freeze-dried PHBV + 15% NFC, Fig. 1(c) shows that some of the PHBV powder attached to the fibrillar NFC network, while some of it aggregated. This PHBV + 15% NFC was used as the masterbatch in the subsequent melt compounding process.

3.2. Tensile properties

Tensile tests were performed on the injection molded ASTM D638 Type V specimens of the PHBV/NFC nanocomposites. Representative stress–strain curves are featured in Fig. 2. Properties such as tensile modulus, tensile strength, and strain-at-break were measured as shown in Table 1. Adding 2.5, 5, and 10 wt% NFC increased the Young's modulus of neat PHBV by 22%, 54%, and 90%, respectively.

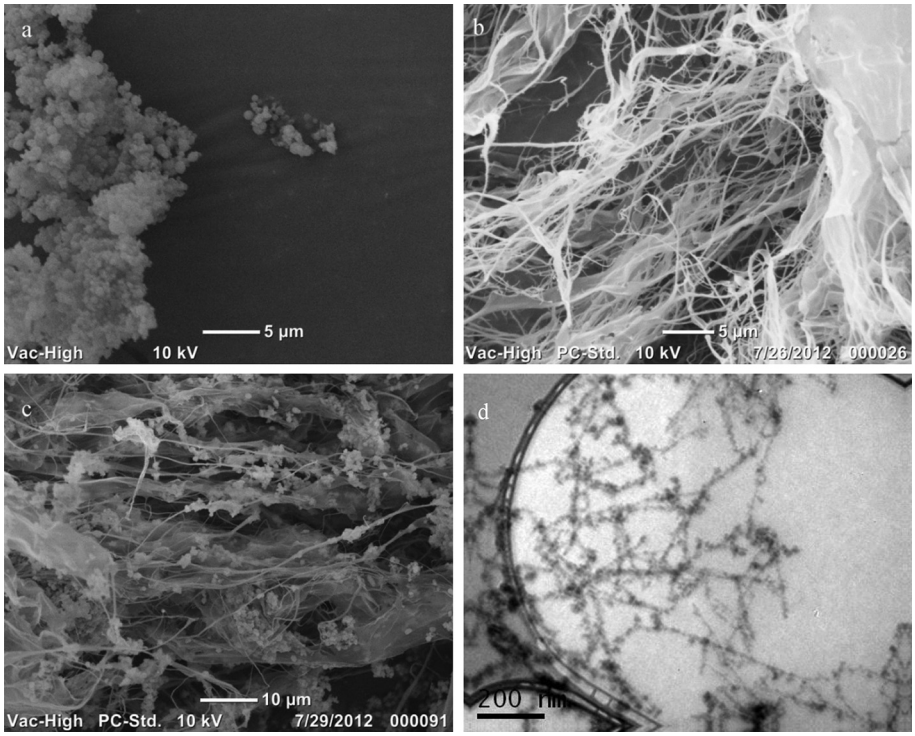

Fig. 1. SEM images of: (a) PHBV powder, (b) freeze-dried NFC, (c) freeze-dried PHBV + 15%NFC, and (d) TEM image of NFC in aqueous gels dried on a TEM grid.

In general, the tensile strength of filled composites was found to be the same as the virgin polymer. Furthermore, the ultimate strain of neat PHBV decreased with increased fiber loading. Maximum elongation decreased more than one-half, from 8.8% for neat PHBV to 3.9% with the addition of 10 wt% NFC. The slight increase in strength and decrease in elongation in the composites might be attributed to an embrittlement caused by some agglomeration of the NFC and nanocomposite degradation. This degradation, which will be discussed later, was further confirmed by DSC, GPC, and TGA results. The SEM micrograph of the tensile fracture surfaces of neat PHBV and PHBV/NFC nanocomposites in Fig. 3 clearly shows that some NFC agglomerated, even though individual fibers with a diameter on the order of 1 μm (cf. Fig. 3(d)) could still be clearly distinguished. Nevertheless, the same phenomena of increasing tensile modulus and decreasing strain-at-break were observed for NFC produced through the same procedure as reinforcement in polymer nanocomposites reported by Bulota et al. [23] and Fujisawa et al. [24].

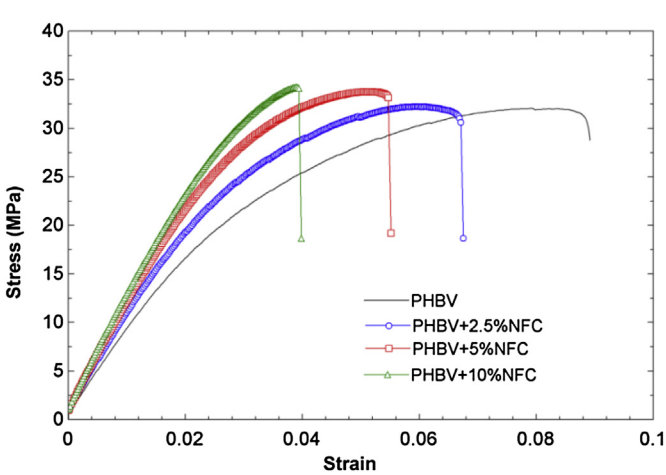

Fig. 2. Tensile stress versus strain curve for NFC and PHBV nanocomposites.

3.3. Thermal properties and calorimetry results

It is well established that fibers and other reinforcements in composites may act as nucleating sites and thus affect the crystallization kinetics of polymeric matrix resins [25]. Thermal properties of PHBV nanocomposites, including crystallization and melting behaviors, were investigated using DSC. Because PHBV has poor thermal stability and undergoes thermal degradation which can lead to a reduction in molecular weight [26,27], two heating and two cooling cycles were performed so that useful comparisons could be made. The heating and cooling cycles are plotted in Figs. 4 and 5 and the results data are listed in Table 2. The data obtained from the first heating cycle include the effect of the prior thermal history of the injection molded samples which underwent rapid cooling during the molding process, thereby impairing the crystallization process of the samples [28]. Upon slow cooling, the second heating cycle had a higher degree of crystallinity than the first heating cycle. There were two competing effects between nucleation and degradation of NFC on PHBV, as described below.

3.3.1. Nucleating effect

Table 2 and Fig. 6 provide clear evidence that NFC served as a nucleating agent. As shown in Table 2, the crystallization

Table 1
Tensile properties of PHBV/NFC nanocomposites.

Sample	Ultimate tensile strength (MPa)	Tensile modulus (MPa)	Strain-at-break
PHBV	31.7 ± 0.3	1681.5 ± 36.2	0.088 ± 0.01
PHBV + 2.5% NFC	32.1 ± 1.0	2064.7 ± 142.6	0.067 ± 0.01
PHBV + 5% NFC	34.4 ± 0.3	2601.4 ± 49.1	0.055 ± 0.004
PHBV + 10% NFC	34.3 ± 0.4	3196.4 ± 87.3	0.039 ± 0.002

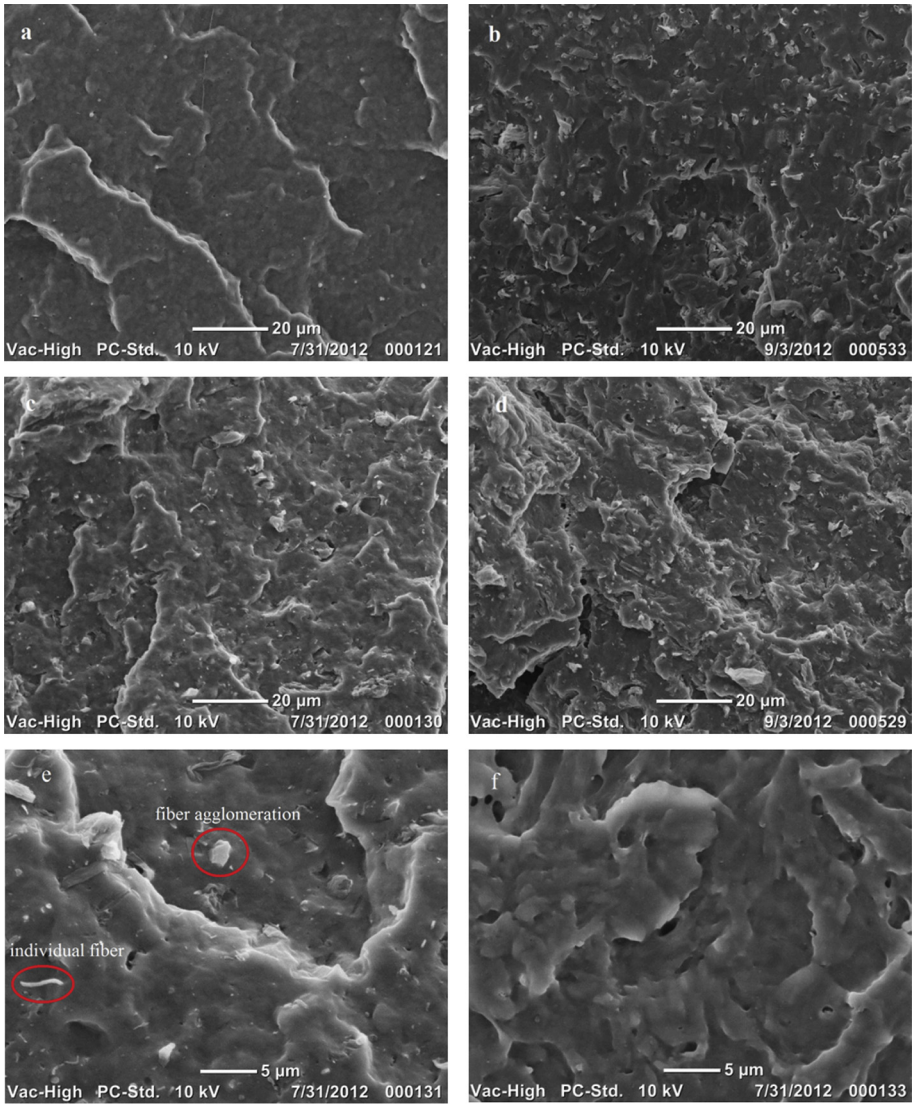

Fig. 3. Tensile fractured surfaces of (a) PHBV, (b) PHBV + 2.5% NFC, (c) PHBV + 5% NFC, (d) PHBV + 10% NFC, (e) higher magnification of Fig. 3c, and (f) higher magnification of Fig. 3a.

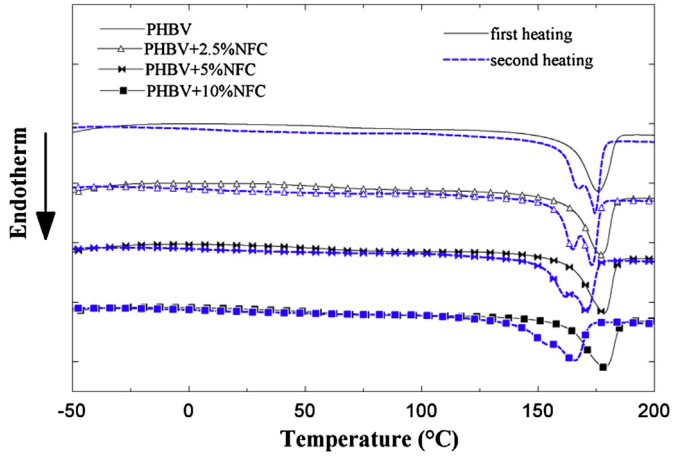

Fig. 4. Comparison of melting endotherms during the first (solid line) and second (dashed line) heating scans of PHBV and its nanocomposites with NFC.

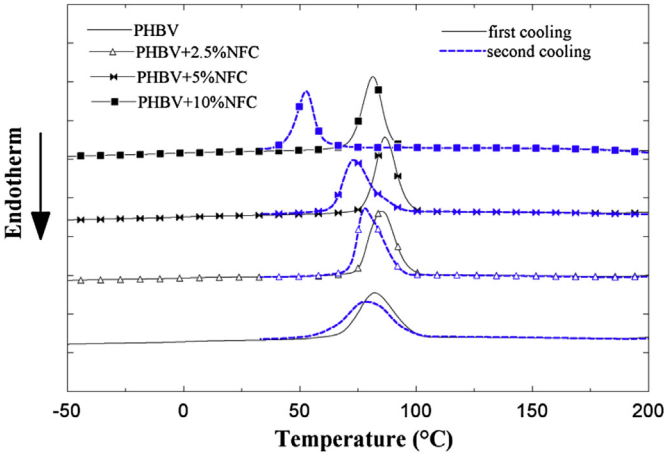

Fig. 5. Comparison of crystallization exotherms during the first (solid line) and second (dashed line) cooling scans of PHBV and its nanocomposites with NFC.

Table 2
Thermal characteristics of PHBV/NFC nanocomposites. The two temperatures in the second heating and second cooling cycle correspond to the two peaks in the DSC curve.

Specimens	Heating				Cooling
	Melting			Degree of crystallinity	Crystallization temperature (°C)
	Temperature (°C)		Enthalpy (J/g)	χ_c (%)	
First heating and first cooling					
PHBV	175.80		79.96	73.35	81.78
PHBV + 2.5% NFC	176.91		79.54	74.84	84.87
PHBV + 5% NFC	178.13		77.95	75.27	86.41
PHBV + 10% NFC	178.46		74.59	76.40	81.85
Second heating and second cooling					
PHBV	167.37	174.35	96.74	88.75	77.11
PHBV + 2.5% NFC	164.92	173.03	94.70	89.10	77.81
PHBV + 5% NFC	161.94	170.75	88.55	85.51	72.85
PHBV + 10% NFC	165.55		78.22	79.73	52.55

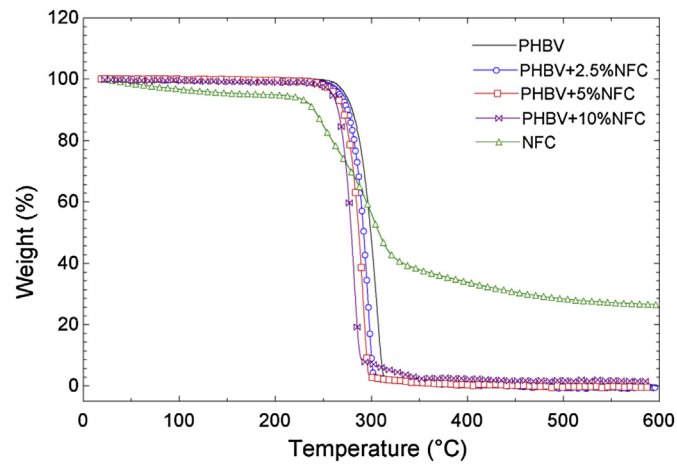

Fig. 7. TGA curves for the PHBV/NFC nanocomposite samples.

temperature (T_c) during the first cooling cycle was higher with the addition of NFC. With the addition of 2.5, 5%, and 10% NFC, the crystallization peak of PHBV was roughly 3 °C, 5 °C, and 0.1 °C higher, respectively. The initial increase and then decrease of crystallization temperatures with increasing NFC content could be the result of two competing factors; namely, enhanced nucleation of crystallization and material degradation due to NFC (to be discussed below). The degree of crystallinity of PHBV slightly increased in the first heating cycle but decreased in the second heating cycle with the addition of NFC (Table 2). This increase in crystallinity was due to the nucleating effect of the nanosized NFC fibers. Similar effects by other nanosized materials on crystallization and degradation have been reported previously [6,29]. The increase in crystallinity of the polymer matrices by the addition of NFC might also increase the tensile modulus of the nanocomposites [30].

Fig. 6 shows the POM photographs of PHBV and PHBV/NFC nanocomposites. For neat PHBV, the number of spherulites was few and their size was relatively large because there was ample space for them to grow before impinging upon one another. For PHBV/NFC nanocomposites, the shape of the spherulites was distorted. Furthermore, their size decreased and the number of PHBV spherulites increased significantly (Fig. 6(b)–(d)). These results confirmed the nucleating effect of NFC. Similar results were reported for PHBV with cellulose nanowhiskers [31] and nanoclay [32].

3.3.2. Degradation during DSC measurement

As shown in Fig. 4, the endothermic peak, which occurred between 160 °C and 180 °C, is referred to as the melting peak of PHBV. An exothermic peak, which occurred between 50 and 100 °C, was observed in all specimens and corresponded to the crystallization of PHBV (cf. Fig. 5). In the DSC test, additional thermal scanning

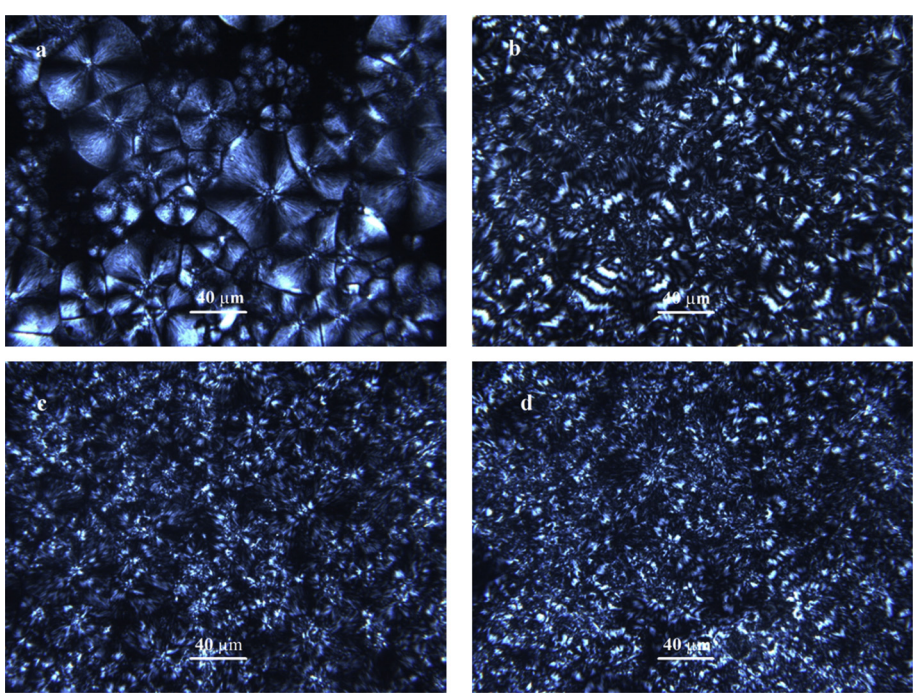

Fig. 6. Polarized optical microscope photographs of PHBV/NFC nanocomposites: (a) PHBV, (b) PHBV + 2.5% NFC, (c) PHBV + 5% NFC, and (d) PHBV + 10% NFC.

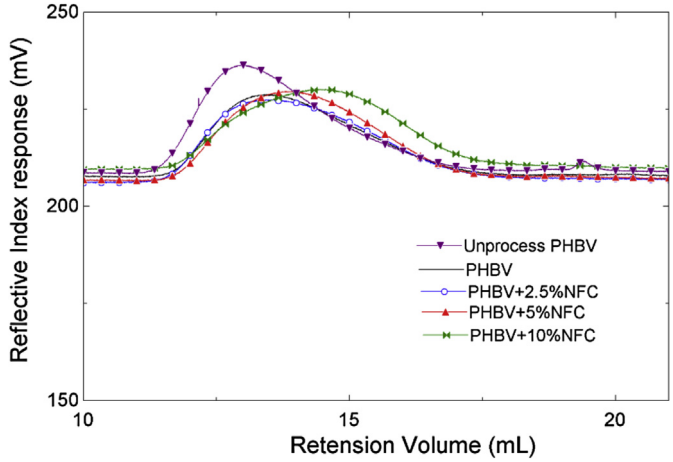

Fig. 8. GPC chromatograms of PHBV/NFC nanocomposite samples.

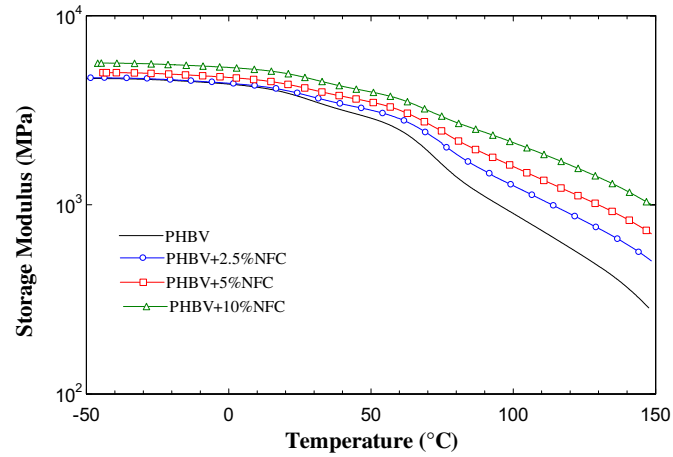

Fig. 9. Storage moduli of the PHBV and PHBV/NFC nanocomposites as a function of temperature.

cycles caused a decrease in the melting (Fig. 4) and crystallization (Fig. 5) temperatures as well as both the melting and crystallization heat suggesting sample degradation. The effect of wood on the thermal degradation of PHBV has been reported [33,34]. The magnitude of the shift increased with increasing NFC concentration, indicating that NFC might cause degradation of the polymer, likely through residual moisture in the NFC, or through the degradation effect of hydroxyl groups on the cellulose from NFC that triggered the PHBV degradation through hydrolysis at high processing temperatures [6,33,35]. An additional step of drying the NFC masterbatch in an oven at 90 °C for 5 h was found to be ineffective in removing the residual moisture, probably due to strong hydrogen bonding between cellulose and water molecules. Further study is needed to remove moisture from the NFC.

3.4. Thermal stability

The thermal stability of the neat PHBV and PHBV/NFC nanocomposite samples were examined using TGA. TGA results shown in Fig. 7 confirm that adding NFC leads to increased degradation. The onset degradation temperature of the PHBV/NFC nanocomposites decreased with the addition of NFC.

For dried NFC, there was an initial and slow weight loss of NFC until around 200 °C, which might be attributed to both the loss of residual moisture in the NFC as well as the slow degradation of NFC. The most pronounced degradation began at approximately 200 °C, which was lower than the maximum temperature of 210 °C used in the heating scans during the DSC analysis. This supports the finding that the material might have degraded at the end of the first DSC heating scan (cf. Fig. 4). Nonetheless, when the maximum temperature used in the DSC was set at 190 °C, heating scan showed similar trend but with lower degree of PHBV degradation. There was an approximate 30% char yield at temperatures above 500 °C.

Table 3
The M_w and PDI of the PHBV powder as received and the four specimens subjected to the mixing and injection molding process.

Samples	M_w	PDI
Unprocessed PHBV	330,000 ± 20,000	2.4
PHBV	260,000 ± 10,000	2.3
PHBV + 2.5% NFC	255,000 ± 10,000	3.4
PHBV + 5% NFC	230,000 ± 9500	3.6
PHBV + 10% NFC	195,000 ± 8000	4.4

3.5. Molecular weight measurement

The M_w and PDI values of the neat PHBV and PHBV/NFC nanocomposites were examined using GPC. GPC results shown in Fig. 8 and Table 3 confirm that adding NFC leads to increased degradation, as mentioned previously. Furthermore, as can be observed, the M_w of the PHBV powder decreased 21% from 330,000 to 260,000 after the mixing and injection molding processes, indicating that the PHBV was prone to thermal degradation during processing [36,37].

3.6. Dynamic mechanical properties

The viscoelastic properties of the PHBV and PHBV/NFC nanocomposites were studied using DMA. The resulting storage moduli and glass transition temperatures in terms of tan-δ of all of the specimens are shown in Figs. 9 and 10, respectively. Below the T_g of the polymer matrix, there was a small increase in modulus, but more significantly, there was a large increase in the modulus above the glass transition temperature of the matrix with the addition of NFC. For example, the modulus for 10 wt% NFC reinforced nanocomposite increased 28% compared to neat PHBV at 25 °C, while the storage modulus increased 137% at a temperature at 100 °C. Similar results for NFC produced through the same procedure as

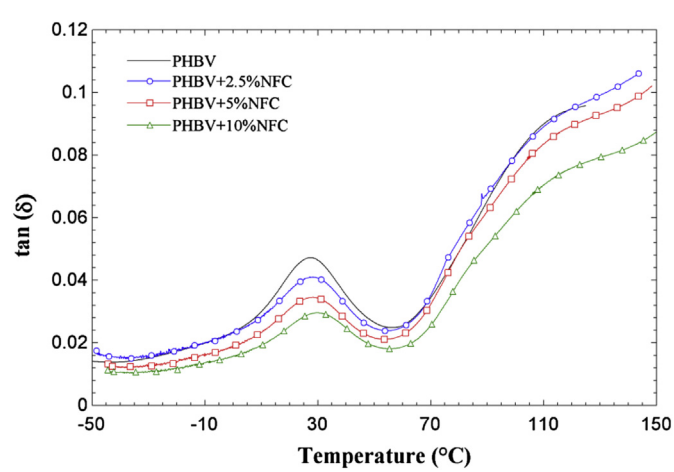

Fig. 10. Tan δ curves of the PHBV and PHBV/NFC nanocomposites.

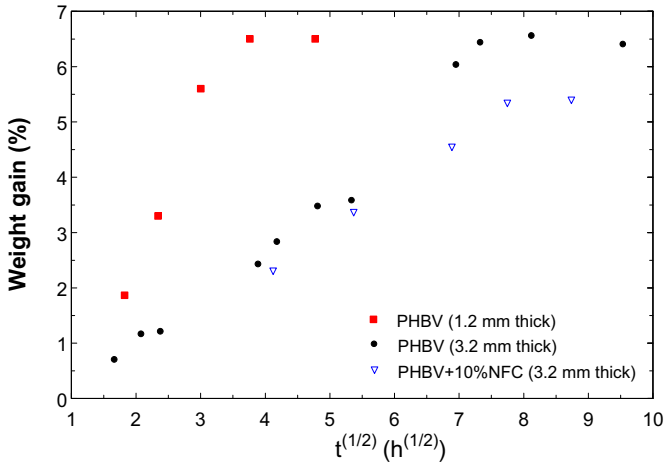

Fig. 11. Absorption curves for CO_2 in PHBV and PHBV/NFC nanocomposites.

reinforcements in polymer nanocomposites have been reported by Besbes et al. [38]; Johnson et al. [39]; Fujisawa et al. 2012 [24] which have attributed this to the formation of a percolated system of cellulose held together by hydrogen bonding at higher temperature.

The glass transition temperature (T_g), which can be obtained from the peaks of the tan-δ curves in Fig. 10, increased with increasing NFC. It was also found that the magnitude of the relaxation process strongly decreased with increasing NFC content and a slight shift of the peak position was observed upon the addition of NFC, which can be attributed to the limitation of chain mobility within the polymer matrix [6,30].

3.7. Sorption behavior of CO_2 in PHBV/NFC nanocomposites

It is known that the foamability of polymers is affected by the sorption of gas in the polymer and that the mechanisms of cell nucleation and cell growth are influenced by the amount of the gas dissolved in the polymer and the rate of gas diffusion [40]. Injection molded PHBV and PHBV/NFC nanocomposite specimens were originally weighed and then placed in a pressure vessel filled with CO_2. After depressurization, they were again placed on the scale to determine the amount of CO_2 absorbed. The weight gain was defined as the ratio between the mass of CO_2 in the sample and the original mass of PHBV. The mass loss described the mass of CO_2 present in the specimen as a function of time after the pressure release. A separate sorption test on NFC fibers alone revealed that the solubility of CO_2 in NFC fibers was negligible. Hence, the absorption and desorption results shown below were adjusted by the weight fraction of PHBV in the nanocomposites.

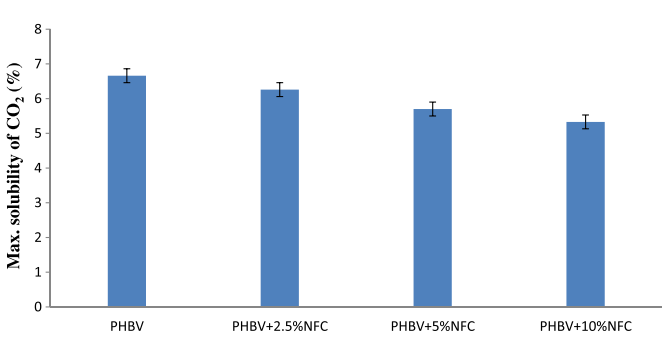

Fig. 12. Maximum solubility of CO_2 in PHBV and their nanocomposites with 2.5, 5, and 10 wt% NFC.

Table 4
Comparison of maximum sorption degree and desorption and sorption coefficients for the different NFC contents.

	PHBV maximum sorption degree (%)	PHBV desorption diffusion coefficient (cm^2/s)	PHBV sorption diffusion coefficient (cm^2/s)
PHBV	6.66	1.15×10^{-7}	6.44×10^{-8}
PHBV + 2.5% NFC	6.26	1.26×10^{-7}	6.06×10^{-8}
PHBV + 5% NFC	5.70	1.54×10^{-7}	5.12×10^{-8}
PHBV + 10% NFC	5.33	2.72×10^{-7}	4.88×10^{-8}

Fig. 11 shows the absorption curves where the weight gain is plotted as a function of the square root of time. Regarding NFC content, the weight gain increased as the specimen thickness decreased. Equilibrium was reached after 50 h of exposure for 3.2 mm thick specimens, and only 16 h for 1.2 mm thick specimens. Nevertheless, the relationship between weight gain and $t^{1/2}$ was initially linear as described in Eq. (2). The sorption amount increased with time of exposure until an equilibrium was reached.

At the same sample thickness, the absorption rate and maximum absorption degree was slightly lower as NFC was added. The maximum sorption degree was plotted as a function of NFC content (Fig. 12). The measured solubility of gas decreased with the addition of NFC in the polymer matrix, perhaps because of the high crystallinity of the fiber as well as a higher degree of crystallinity of PHBV acting as a CO_2 barrier, as suggested by Matuana and Park et al. [12,19,41]. The results obtained are presented in Table 4 and summarize the maximum absorption degree and absorption coefficients estimated from the curve in Fig. 11 and Eq. (2) for the different experiments performed.

Similar to the absorption behavior, the rate of weight loss increased as sample thickness decreased. However, to compare the influence of NFC on the desorption behavior, 1.2 mm thick injection molded specimens were used. The desorption curves for CO_2 in neat PHBV and PHBV/NFC nanocomposite specimens around one to 2 h are illustrated in Fig. 13. The fractional mass loss of CO_2 was approximated by a linear relationship with $t^{1/2}$ and the slope became steeper as the NFC content increased. Hence, the desorption diffusivity also increased as the amount of NFC increased. The increase in desorption diffusivity with an increasing fiber content might be due to the lower molecular weight (as a result of degradation) in the NFC nanocomposite as well as

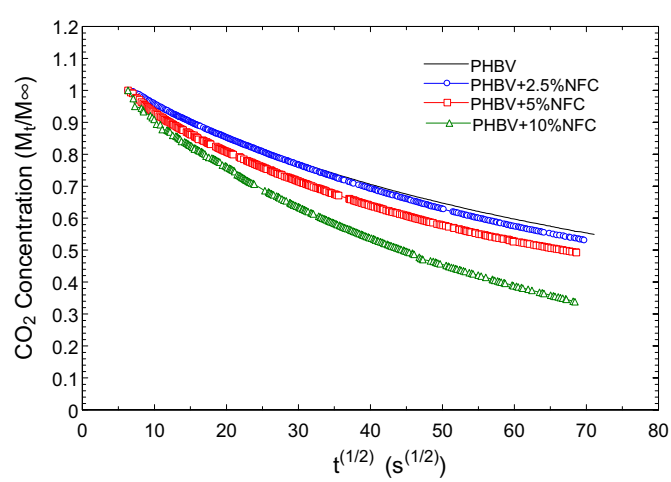

Fig. 13. Desorption curves for CO_2 in PHBV and PHBV/NFC nanocomposites.

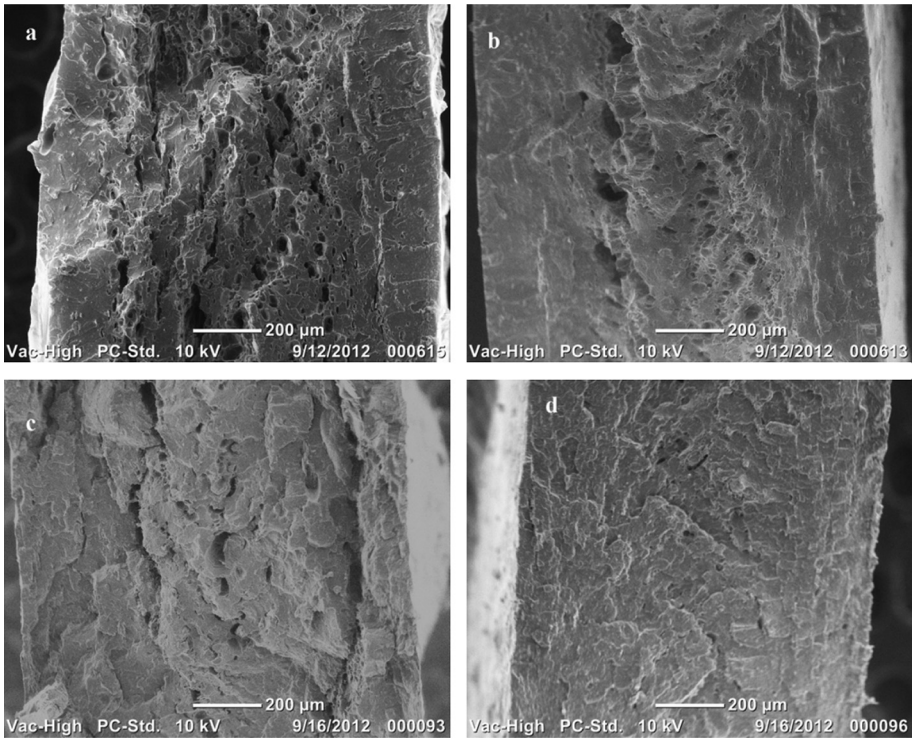

Fig. 14. SEM images of foamed PHBV and PHBV/NFC nanocomposites at 155 °C for 1 min: (a) PHBV, (b) PHBV + 2.5% NFC, (c) PHBV + 5% NFC, and (d) PHBV + 10% NFC.

the interface between fibers and matrix that provide a channel through which gas can quickly escape from the composites as reported in Refs. [12,40].

Moreover, as shown in Table 4, the experiments led to higher values for the desorption diffusion coefficient than for the sorption diffusion coefficient. It was suggested that the plasticizing effect of CO_2 was responsible for this tendency [11]. Even though sorption took place under higher pressure conditions and desorption proceeded at ambient temperature and pressure, the release of CO_2 from the polymer matrix during desorption was faster due to the higher chain mobility of the polymer substrate, which had been exposed to high pressure and temperature.

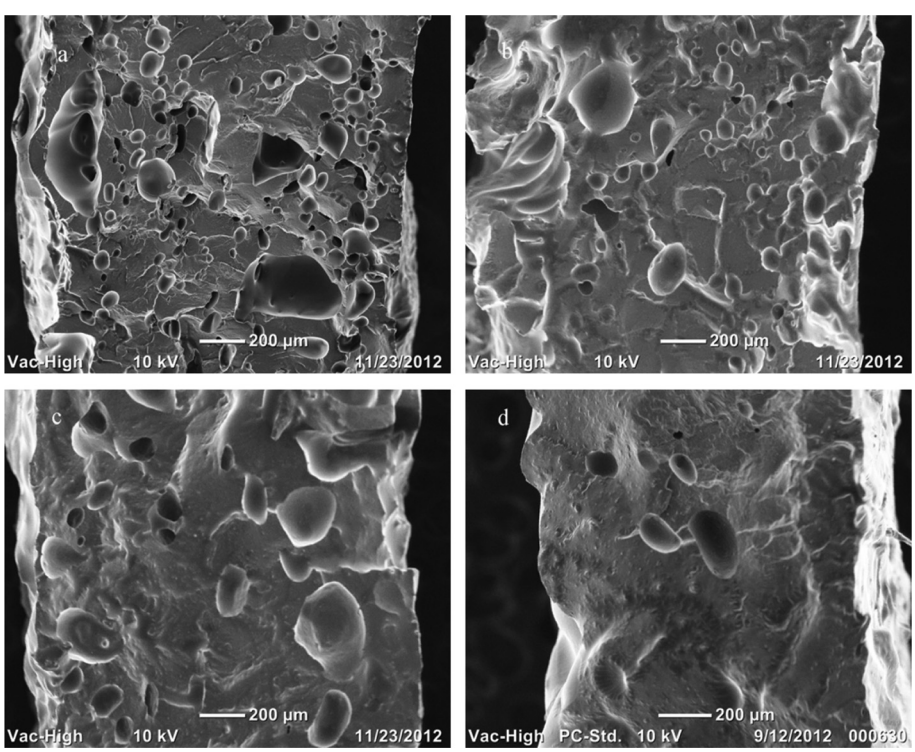

Fig. 15. SEM images of foamed PHBV and PHBV/NFC nanocomposites at 175 °C for 1 min: (a) PHBV, (b) PHBV + 2.5% NFC, (c) PHBV + 5% NFC, and (d) PHBV + 10% NFC.

3.8. Foamed PVOH/NFC nanocomposites

To investigate their foaming behavior, CO_2-saturated specimens were placed in a hot oil bath at various temperatures for 1 min after removal from the CO_2 pressure vessel. Since thinner specimens had less temperature variations within the specimen, specimens 1.2 mm thick were used to study the effect of NFC on foaming behavior. When the polymer/gas solution was heated in the hot oil bath, the stiffness of the polymer matrix decreased, the gas diffusion rate increased, and the cells began to grow. The volume of the foaming specimens increased as the cells continued to grow, as driven by the gas molecules diffusing into the nucleated cells from the polymer matrix [19].

No foamed structure (hence no cells) was seen at a hot oil bath temperature below 140 °C. Cellular morphology developed in nanocomposites that foamed at a hot oil bath temperature of 155 and 175 °C, as illustrated in Figs. 14 and 15, respectively. At the end of foaming, the foamed samples were frozen in liquid nitrogen and then quickly fractured. As shown in the figures, increasing the foaming temperature resulted in a significant increase in cell size. Higher temperatures accelerated the rate of gas diffusion and softened the polymer, which favored cell growth [19]. However, the void fraction decreased when NFC was added to the polymer matrix. It is because the addition of NFC decreased the solubility of CO_2, accelerated the gas loss during foaming (cf. Fig. 13), increased PHBV strength at high temperature (cf. Fig. 9), and increased the degree of crystallinity (cf. Table 2) as suggested by Park et al. [12]. Therefore, development of foamed structures and a high porosity were adversely affected by adding the NFC. Similar results have been reported in several other studies on wood fiber-filled polymers [40,42]. More studies are needed to more precisely quantify the effect of NFC on the foaming behavior of PHBV.

4. Conclusions

Cellulose nanocomposite processing via a masterbatch with a high content of NFC in PHBV—a process which is scalable from the laboratory to an industrial setting—was attempted. The NFC and PHBV powders were pre-mixed, freeze-dried, and melt compounded to obtain nanocomposites with different fiber compositions. NFC increased the modulus of PHBV, as observed via both DMA and tensile tests. However, toughness decreased as the amount of NFC increased. The addition of NFC to PHBV was shown to increase the crystallization and glass transition temperatures, but also caused the thermal degradation of PHBV, likely due to residual moisture or other components such as the hydroxyl group in the NFC. The absorption degree of CO_2 in the nanocomposites decreased and the desorption diffusivity increased as more NFC was added. Finally, the addition of NFC inhibited the foaming ability due to less CO_2 sorption, fast CO_2 loss, and a higher degree of crystallinity.

Acknowledgments

The financial support of the USDA National Institute of Food and Agriculture Award (No. 2011-67009-20056) is gratefully acknowledged in this research. The authors would also like to thank Sara Fishwild of the Forest Products Laboratory for performing the tensile tests, Dr. Rick Reiner of the Forest Products Laboratory for preparing cellulose nanofibers, and Jun Peng for his useful advice.

References

[1] Mohanty A, Misra M, Drzal L. Sustainable bio-composites from renewable resources: opportunities and challenges in the green materials world. J Polym Environ 2002;10:19–26.
[2] Javadi A, Srithep Y, Lee J, Pilla S, Clemons C, Gong S, et al. Processing and characterization of solid and microcellular PHBV/PBAT blend and its RWF/nanoclay composites. Compos Part A: Appl Sci Manuf 2010;41:982–90.
[3] Ten E, Turtle J, Bahr D, Jiang L, Wolcott M. Thermal and mechanical properties of poly (3-hydroxybutyrate-*co*-3-hydroxyvalerate)/cellulose nanowhiskers composites. Polymer 2010;51:2652–60.
[4] Reinsch VE, Kelley SS. Crystallization of poly (hydroxybutrate *co* hydroxyvalerate) in wood fiber reinforced composites. J Appl Polym Sci 1998;64:1785–96.
[5] Doi Y, Tamaki A, Kunioka M, Soga K. Production of copolyesters of 3-hydroxybutyrate and 3-hydroxyvalerate by Alcaligenes eutrophus from butyric and pentanoic acids. Appl Microbiol Biotechnol 1988;28:330–4.
[6] Srithep Y, Turng LS, Sabo R, Clemons C. Nanofibrillated cellulose (NFC) reinforced polyvinyl alcohol (PVOH) nanocomposites: properties, solubility of carbon dioxide, and foaming. Cellulose 2012:1–15.
[7] Siqueira G, Bras J, Dufresne A. Cellulosic bionanocomposites: a review of preparation, properties and applications. Polymers 2010;2:728–65.
[8] Dufresne A, Cavaille JY, Vignon MR. Mechanical behavior of sheets prepared from sugar beet cellulose microfibrils. J Appl Polym Sci 1997;64:1185–94.
[9] Jonoobi M, Harun J, Mathew AP, Oksman K. Mechanical properties of cellulose nanofiber (CNF) reinforced polylactic acid (PLA) prepared by twin screw extrusion. Compos Sci Technol 2010;70:1742–7.
[10] Oksman K, Mathew A, Bondeson D, Kvien I. Manufacturing process of cellulose whiskers/polylactic acid nanocomposites. Compos Sci Technol 2006;66:2776–84.
[11] Cravo C, Duarte ARC, Duarte CMM. Solubility of carbon dioxide in a natural biodegradable polymer: determination of diffusion coefficients. J Supercrit Fluids 2007;40:194–9.
[12] Doroudiani S, Park CB, Kortschot MT. Effect of the crystallinity and morphology on the microcellular foam structure of semicrystalline polymers. Polym Eng Sci 1996;36:2645–62.
[13] Cheung H, Ho M, Lau K, Cardona F, Hui D. Natural fibre-reinforced composites for bioengineering and environmental engineering applications. Compos Part B: Eng 2009;40:655–63.
[14] Javadi A, Srithep Y, Pilla S, Lee J, Gong S, Turng LS. Processing and characterization of solid and microcellular PHBV/coir fiber composites. Mater Sci Eng C 2010;30:749–57.
[15] Saito T, Nishiyama Y, Putaux JL, Vignon M, Isogai A. Homogeneous suspensions of individualized microfibrils from TEMPO-catalyzed oxidation of native cellulose. Biomacromolecules 2006;7:1687–91.
[16] Pääkkö M, Vapaavuori J, Silvennoinen R, Kosonen H, Ankerfors M, Lindström T, et al. Long and entangled native cellulose I nanofibers allow flexible aerogels and hierarchically porous templates for functionalities. Soft Matter 2008;4:2492–9.
[17] Standard test method for tensile properties of plastics. ASTM D638-10: ASTM International.
[18] Matuana L. Solid state microcellular foamed poly (lactic acid): morphology and property characterization. Bioresour Technol 2008;99:3643–50.
[19] Matuana LM, Park CB, Balatinecz JJ. Processing and cell morphology relationships for microcellular foamed PVC/wood-fiber composites. Polym Eng Sci 1997;37:1137–47.
[20] Vieth WR. Diffusion in and through polymers: principles and applications. Hanser Munich; 1991.
[21] Crank J. The mathematics of diffusion 1979.
[22] Baldwin DF, Park CB, Suh NP. A microcellular processing study of poly (ethylene terephthalate) in the amorphous and semicrystalline states. Part I: Microcell nucleation. Polym Eng Sci 2004;36:1437–45.
[23] Bulota M, Hughes M. Toughening mechanisms in poly (lactic) acid reinforced with TEMPO-oxidized cellulose. J Mater Sci 2012:1–7.
[24] Fujisawa S, Ikeuchi T, Takeuchi M, Saito T, Isogai A. Superior reinforcement effect of TEMPO-oxidized cellulose nanofibrils in polystyrene matrix: optical, thermal, and mechanical studies. Biomacromolecules 2012;13:2188–94.
[25] Quan H, Li ZM, Yang MB, Huang R. On transcrystallinity in semi-crystalline polymer composites. Compos Sci Technol 2005;65:999–1021.
[26] Pilla S. Handbook of bioplastics and biocomposites engineering applications. Wiley-Scrivener; 2011.
[27] Avella M, Martuscelli E, Raimo M. Review properties of blends and composites based on poly (3-hydroxy) butyrate (PHB) and poly (3-hydroxybutyrate-hydroxyvalerate)(PHBV) copolymers. J Mater Sci 2000;35:523–45.
[28] Srithep Y, Javadi A, Pilla S, Turng LS, Gong S, Clemons C, et al. Processing and characterization of recycled poly (ethylene terephthalate) blends with chain extenders, thermoplastic elastomer, and/or poly (butylene adipate-*co*-terephthalate). Polym Eng Sci 2011;51:1023–32.
[29] Probst O, Moore EM, Resasco DE, Grady BP. Nucleation of polyvinyl alcohol crystallization by single-walled carbon nanotubes. Polymer 2004;45:4437–43.
[30] Srithep Y, Nealey P, Turng LS. Effects of annealing time and temperature on the crystallinity and heat resistance behavior of injection molded poly (lactic acid). Polym Eng Sci 2012.
[31] Ten E, Jiang L, Wolcott MP. Crystallization kinetics of poly (3-hydroxybutyrate-*co*-3-hydroxyvalerate)/cellulose nanowhiskers composites. Carbohyd Polym 2012.
[32] Wang S, Song C, Chen G, Guo T, Liu J, Zhang B, et al. Characteristics and biodegradation properties of poly (3-hydroxybutyrate-*co*-3-hydroxyvalerate)/organophilic montmorillonite (PHBV/OMMT) nanocomposite. Polym Degrad Stabil 2005;87:69–76.
[33] Singh S, Mohanty A. Wood fiber reinforced bacterial bioplastic composites: fabrication and performance evaluation. Compos Sci Technol 2007;67:1753–63.

[34] Fernandes EG, Pietrini M, Chiellini E. Bio-based polymeric composites comprising wood flour as filler. Biomacromolecules 2004;5:1200–5.
[35] Pilla S, Gong S, O'Neill E, Yang L, Rowell RM. Polylactide recycled wood fiber composites. J Appl Polym Sci 2008;111:37–47.
[36] Smith R. Biodegradable polymers for industrial applications. CRC; 2005.
[37] Lai M, Li J, Yang J, Liu J, Tong X, Cheng H. The morphology and thermal properties of multi-walled carbon nanotube and poly (hydroxybutyrate-*co*-hydroxyvalerate) composite. Polym Int 2004;53:1479–84.
[38] Besbes I, Vilar MR, Boufi S. Nanofibrillated cellulose from Alfa, Eucalyptus and Pine fibres: preparation, characteristics and reinforcing potential. Carbohydr Polym 2011;86:1198–206.
[39] Johnson RK, Zink-Sharp A, Renneckar SH, Glasser WG. A new bio-based nanocomposite: fibrillated TEMPO-oxidized celluloses in hydroxypropylcellulose matrix. Cellulose 2009;16:227–38.
[40] Rachtanapun P, Selke S, Matuana L. Microcellular foam of polymer blends of HDPE/PP and their composites with wood fiber. J Appl Polym Sci 2003;88:2842–50.
[41] Matuana LM, Park CB, Balatinecz JJ. Cell morphology and property relationships of microcellular foamed PVC/wood fiber composites. Polym Eng Sci 1998;38:1862–72.
[42] Matuana LM, Mengeloglu F. Microcellular foaming of impact modified rigid PVC/wood flour composites. J Vinyl Addit Technol 2004;7:67–75.